Eur. Phys. J. C (2014) 74:3029
DOI 10.1140/epjc/s10052-014-3029-6

THE EUROPEAN PHYSICAL JOURNAL C

Regular Article - Theoretical Physics

QCD analysis of forward neutron production in DIS

Federico Alberto Ceccopieri[a]

IFPA, Université de Liège, Allée du 6 août, Bât B5a, 4000 Liège, Belgium

Received: 9 June 2014 / Accepted: 10 August 2014 / Published online: 28 August 2014

Abstract We consider forward neutron production in DIS within fracture functions formalism. By performing a QCD analysis of available data we extract proton-to-neutron fracture functions exploiting a method which is in close relation with the factorisation theorem for this class of processes.

1 Introduction

In hadronic collisions a portion of the produced particle spectrum is characterised by hadrons carrying a sizeable fraction of the available energy and produced at small polar angle with respect to the collision axis. It is phenomenologically observed that for such hadrons their valence-parton composition is almost or totally conserved with respect to the one of initial-state hadrons [1]. Such semi-inclusive processes allow one to test the scaling hypothesis for forward hadron production cross sections [2,3] and give insight on non-perturbative aspects of QCD dynamics in high energy collisions. These hadrons, in fact, are produced at very small transverse momenta with respect to the collision axis, a regime where perturbative techniques cannot be applied. Quite interestingly, forward particle production has also been observed in processes which involve point-like probes in lepton–hadron interactions, such as Semi-Inclusive Deep Inelastic Scattering (SIDIS). At variance with the hadronic collisions mentioned above, such process involves a large momentum transfer at the lepton vertex. The presence of a hard scale is a basic requirement in the derivation of a dedicated factorisation theorem [4–7] which ensures that collinear QCD factorisation holds in the leading-twist approximation for forward particle production in DIS. The relevant cross sections can then be factorised into perturbatively calculable short-distance cross sections and new distributions, fracture functions, which simultaneously encode information both on the interacting parton and on the non-perturbative QCD dynamics of the spectator fragmentation into the observed forward hadron. In spite of being non-perturbative in nature, their scale dependence can be calculated within perturbative QCD [8]. Fracture functions obey in fact DGLAP [9–11] inhomogeneous evolution equations which result from the structure of collinear singularities in the target-fragmentation region [8,12]. The dedicated factorisation theorem [4–7] guarantees that fracture functions are universal distributions, at least in the context of SIDIS. On this theoretical basis, an impressive experimental program has been pursued at HERA in diffractive DIS which led to accurate determination of the so-called diffractive parton distributions, i.e. proton-to-proton fracture functions in the very forward limit, allowing for the first time a quite accurate investigation of the parton content of the pomeron. The whole formalism has been later used in Ref. [13] to extract proton-to-Lambda fracture functions within a combined perturbative QCD fit to available SIDIS data.

In this paper we will focus on forward neutron production in DIS which provides, with respect to the aforementioned processes, complementary informations on soft QCD dynamics. An intensive physics program with forward neutron tagging has been pursued at HERA as well, where recent results [14,15] show that around 8 % of the DIS events contain a forward neutron. These data are crucial in testing the limiting fragmentation hypothesis [16] and have been used as benchmark in a number of Regge-based models [17–23] which mainly concentrate on the modelisation of forward neutron production mechanisms. In the present paper we adopt instead a complementary approach and no modelisation of neutron production mechanisms is attempted. This strategy is consistent with the factorisation theorem. The resulting set of proton-to-neutron fracture functions (nFFs) could then be used in hard-scattering factorisation tests [24] in forward neutron tagged dijet photoproduction in ep collisions, as already measured at HERA [25,26], where factorisation is expected to hold only for the so-called direct component of the cross section. Even more intriguing appears to

[a] e-mail: federico.ceccopieri@hotmail.it

be the possibility of using nFFs for predicting the cross section for the associated production of a forward neutron and a Drell–Yan pair or dijet system in hadronic collisions. For this processes the factorisation theorem is not expected to hold and therefore nFFs determined by DIS data alone offer the opportunity to gauge factorisation breaking effects.

The paper is organised as follows. In Sect. 2 we describe the process under study, the kinematic variables relevant to the analysis and the observable used in the fit. In Sect. 3 we discuss the evolution of fracture functions and the general method with which we build initial conditions for the QCD evolution. In Sect. 4 we describe the details of the QCD fit and in Sect. 5 we assess the impact of experimental and theoretical errors on the obtained neutron FF set. In Sect. 6 we summarise our results.

2 Data set and observable

In this analysis we consider semi-inclusive DIS events of the type

$$e^+(k) + p(P) \to e^+(k') + n(P_n) + X(p_X), \tag{1}$$

where, beside the outgoing lepton, an additional neutron n is detected in the final state. In Eq. (1) X stands for the unobserved part of the hadronic system and particles four-momenta are indicated in parenthesis. The kinematic variables Q^2, x_B and y are used to describe the inclusive DIS scattering process. They are defined as

$$q = k - k', \quad Q^2 = -q^2, \quad x_B = \frac{Q^2}{2P\cdot q}, \quad y = \frac{P\cdot q}{P\cdot k}. \tag{2}$$

The kinematic variables used to describe the final state neutron are the neutron transverse momentum p_T evaluated with respect to the beam axis and the longitudinal momentum fraction x_L defined by

$$x_L = 1 - \frac{q\cdot(P - P_n)}{P\cdot q} \simeq E_n/E_p, \tag{3}$$

where E_n and E_p are the neutron and proton energy in the laboratory frame, respectively. In the following we use the scaled fractional momentum variable β defined by

$$\beta = \frac{x_B}{1 - x_L}, \tag{4}$$

where $1-x_L$ is the maximum available fractional momentum of the parton participating in the hard scattering. The analysis is performed on the H1 ep data of Ref. [27] with positrons and protons energies, respectively, of $E_e = 27.6$ GeV and $E_p = 920$ GeV, corresponding to a centre-of-mass energy of $\sqrt{s} = 319$ GeV. The kinematic range of the selected DIS events is $6 < Q^2 < 100\ \mathrm{GeV}^2$, $0.02 < y < 0.6$ and $1.5\cdot10^{-4} < x_B < 3\cdot10^{-2}$. The values of x_L range from 0.365 to 0.905. The kinematic β-coverage is x_L-dependent, in particular $\beta_{\min} = 3.52\cdot10^{-4}$ at $x_L = 0.365$ and $\beta_{\max} = 0.22$ at $x_L = 0.905$. Forward neutron production is characterised by small values of p_T. In Ref. [27] an upper limit on p_T is used to define the semi-inclusive forward neutron cross section which is correspondingly integrated up to $p_{T,\max} = 0.2$ GeV. Data are presented as a threefold reduced e^+p cross section, $\sigma_r^{LN(3)}$, which depends on the leading neutron transverse and longitudinal structure functions $F_2^{LN(3)}$ and $F_L^{LN(3)}$, respectively. In the one-photon exchange approximation, it reads

$$\sigma_r^{LN(3)}(\beta, Q^2, x_L) = F_2^{LN(3)}(\beta, Q^2, x_L) - \frac{y^2}{1+(1-y)^2} F_L^{LN(3)}(\beta, Q^2, x_L). \tag{5}$$

3 Theory setup

Hard-scattering factorisation for this class of processes states that the structure functions in Eq. (5) are of the form

$$F_k^{LN(3)}(\beta, Q^2, x_L, p_T^2) = \sum_i \int_\beta^1 \frac{d\xi}{\xi}\, M_{i/P}^N(\beta, \mu_F^2; x_L, p_T^2) \times C_{ki}\left(\frac{\beta}{\xi}, \frac{Q^2}{\mu_F^2}, \alpha_s(\mu_R^2)\right) + \mathcal{O}\left(\frac{1}{Q^2}\right). \tag{6}$$

The index i runs on the flavour of the interacting parton. The hard-scattering coefficients C_{ki} ($k = 2, L$) are perturbatively calculable as a power expansion in the strong coupling α_s and depend upon μ_F^2 and μ_R^2, the factorisation and renormalisation scales, respectively. The C_{ki} coefficient functions are the same as in fully inclusive DIS. The proton-to-neutron fracture functions $M_{i/P}^N(\beta, \mu_F^2, x_L, p_T^2)$ can be interpreted as the number density of interacting partons at a scale μ_F^2 and fractional momentum β conditional to the observation of a forward neutron in the final state specified by a fractional momentum x_L and transverse momentum squared p_T^2. They contain non-perturbative information on the fragmentation of the spectator system which results from the hard interactions. The p_T-unintegrated nFFs appearing in Eq. (6) obey standard DGLAP [9–11] evolution equations [28]. In the case p_T is integrated over up to values of order Q^2, neutron fracture functions obey an inhomogeneous DGLAP-type evolution equations [8]. The additional inhomogeneous term takes into account neutron production from the fragmentation of initial state parton radiation. In the present case, where the p_T of the neutron is integrated up to some $p_{T,\max}$ which lies in the non-perturbative region, neutron fracture functions are defined as

$$M_{i/P}^N(\beta, Q^2, x_L) = \int^{p_{T,\max}^2} dp_T^2\, M_{i/P}^N(\beta, Q^2, x_L, p_T^2) \tag{7}$$

and again obey familiar DGLAP evolution equations [29]

$$Q^2 \frac{\partial M^N_{i/P}(\beta, Q^2, x_L)}{\partial Q^2} = \frac{\alpha_s(Q^2)}{2\pi} \int_\beta^1 \frac{du}{u} P_i^j(u)\, M^N_{j/P}\Big(\frac{\beta}{u}, Q^2, x_L\Big), \quad (8)$$

valid at fixed values of x_L. The central problem of this type of analyses is to find sensible initial conditions for the relevant distributions prior to evolution. It is indeed possible to use phenomenological models to describe forward neutron production. In general at low and intermediate x_L the dominant mechanism is expected to be proton-remnant fragmentation into neutrons, while at high x_L the exchange of virtual particles is expected to dominate. On the other hand, in the present analysis, we work at fixed x_L and no attempts are made to model this non-perturbative dynamics at the proton vertex. Since hard-scattering factorisation in the form Eq. (6) holds at fixed values of x_L and p_T^2 and this dependence is fully contained in nFFs, these conditional parton distributions are exclusively fixed by the kinematics of the outgoing neutron and they are, at least in principle, different for different values of x_L and p_T^2. The approach we describe in this paper fully takes into account these important recipes in the construction of sensible input for nFFs distributions focusing on parton dynamics as explored by the virtual photon once an additional forward neutron is detected in the final state. This new approach has already been used in the extraction of diffractive parton densities from diffractive DIS data in Ref. [30]. This idea is realised in practice performing a series of QCD fits at fixed values of x_L with a common initial condition controlled by a set of parameters $\{p_i\}$. This procedure guide us to deduce the approximate dependence of parameters $\{p_i\}$ on x_L allowing the construction of a generalised initial condition in the (β, x_L)-space to be used in a x_L-combined QCD fit. This procedure can be generalised to take into account the p_T dependence. In particular, if four-differential cross sections were available, we could test whether, at fixed x_L, the parton content probed by the virtual photon is the same (apart from normalisation) in different neutron p_T ranges.

4 Fitting procedure

In this section we describe QCD fits at fixed values of x_L. The distributions of neutron FFs in the quark sector at large β could show valence-like structures for some quark-flavour combinations. However, the accessible values of β in the experimental data are quite low. In view of this fact, and in order to reduce the number of free parameters, we assume that all light quark distributions are equal to each other, so that only the singlet and gluon distributions are required. We assume for the latter, at the arbitrary scale Q_0^2 and for any given value of x_L, a momentum distributions of the type:

$$\beta\, M^N_{\Sigma/P}(\beta, Q_0^2) = A_q\, \beta^{B_q}\, (1-\beta)^{C_q}, \quad (9)$$

$$\beta\, M^N_{g/P}(\beta, Q_0^2) = A_g\, \beta^{B_g}\, (1-\beta)^{C_g}. \quad (10)$$

These distributions are then evolved with the QCDNUM17 [31] package within a zero mass (ZM) variable flavour number scheme (VFNS) at next-to-leading order. Within this scheme heavy flavours distributions are generated radiatively above their respective mass thresholds which are set to $m_c = 1.4$ GeV and $m_b = 4.5$ GeV for charm and bottom quark, respectively. In the VFNS the initial conditions must be imposed at $Q_0^2 < m_c^2$. The factorisation and renormalisation scale are both set equal to Q^2. The coupling constant is set to $\alpha_s(M_Z^2) = 0.118$. The convolution engine of QCDNUM17 is used to obtain $F_2^{LN(3)}$ and $F_L^{LN(3)}$ structure functions at next-to-leading order which are then used to calculate the reduced cross section in Eq. (5) and minimised against data by using the MINUIT program [32]. We adopt the generalised χ^2 definition proposed in Ref. [33]

$$\chi^2 = \sum_i \left(\frac{m_i - f_i(\mathbf{p}, \mathbf{s})}{\sigma_i}\right)^2 + \sum_k s_k^2, \quad (11)$$

where systematics effects are incorporated in theory model predictions

$$f_i(\mathbf{p}, \mathbf{s}) = t_i(\mathbf{p}) + \sum_k s_k \Delta_{ik}. \quad (12)$$

In the above formulae, m_i is the measurement of data point i, t_i is the model prediction depending on a set of parameters $\mathbf{p}$, σ_i are the uncorrelated and statistical errors on data point i added in quadrature and Δ_{ik} is the correlated systematic error from source k on the data i. The variables s_k denote Gaussian random variables with zero mean and unit variance. In the present Section we use the above definitions with $s_k = 0$.

No cut on the invariant mass of the hadronic system X nor on the minimum Q^2 of data to be included in the fit is applied. As already discussed above, given the kinematic coverage of the data, we found that the singlet large-β coefficient C_q is loosely constrained by data. For the gluon distribution, which is only indirectly constrained by scaling violations, we found that B_g strongly correlates with A_g, when the former is left free to vary in the fit. Therefore we set tentatively $C_q = 0.5$, $C_g = 1$ and $B_g = 0$ so that the initial condition contains three free parameters in each x_L-bin. We performed a combined scan on the value of initial scale Q_0^2. Given the quite stiff functional form of the initial conditions, there is a mild dependence of the χ^2 on Q_0^2 which is then fixed at $Q_0^2 = 1$ GeV^2. An essential condition for the x_L-combination procedure to work is that good quality fits must be obtained in each x_L-bin with the common initial conditions, Eqs. (9, 10). The χ^2 values of the fixed-x_L fits, obtained with statistical and uncorrelated uncertainties added in quadrature, are

Table 1 χ^2 values for fits at fixed values of x_L with initial condition in Eqs. (9, 10). The total χ^2, calculated as the sum of partial χ^2 at fixed x_L, and the total number of fitted points are also indicated

x_L	χ^2	Fitted points
0.365	12.0	29
0.455	25.5	29
0.545	19.9	29
0.635	21.0	29
0.725	23.6	29
0.815	17.1	29
0.905	15.7	29
Sum	134.8	203

Table 2 χ^2 values for the combined-x_L fit. In the third column is indicated the χ^2 difference between combined-x_L and fixed-x_L fits in each x_L-bin. The total χ^2 of the combined-x_L fit and the combination penalty are also indicated

x_L	χ^2	$\Delta\chi^2$
0.3650	12.7	+0.7
0.4550	27.5	+2.0
0.5450	22.0	+2.1
0.6350	22.3	+1.3
0.7250	25.5	+1.9
0.8150	17.3	+0.2
0.9050	16.3	+0.6
Tot	143.6	+8.8

presented in Table 1. From these values we may conclude that initial conditions provided by Eqs. (9, 10), supplemented by the constraints on C_q, C_g and B_g, are general enough to describe the data in all x_L-bins. With these results at hand we may now proceed and discuss the x_L-combined fit. The generalised initial conditions have now the form

$$\begin{aligned}\beta\, M^N_{\Sigma/P}(\beta, Q_0^2, x_L) &= A_q(x_L)\, \beta^{B_q(x_L)}\, (1-\beta)^{C_q(x_L)},\\ \beta\, M^N_{g/P}(\beta, Q_0^2, x_L) &= A_g(x_L)\, \beta^{B_g(x_L)}\, (1-\beta)^{C_g(x_L)},\end{aligned} \quad (13)$$

where the β dependence is the same as in Eqs. (9, 10) and the various coefficients are now x_L-dependent. The dependences of the A_q, B_q and A_g free parameters on x_L may be inferred

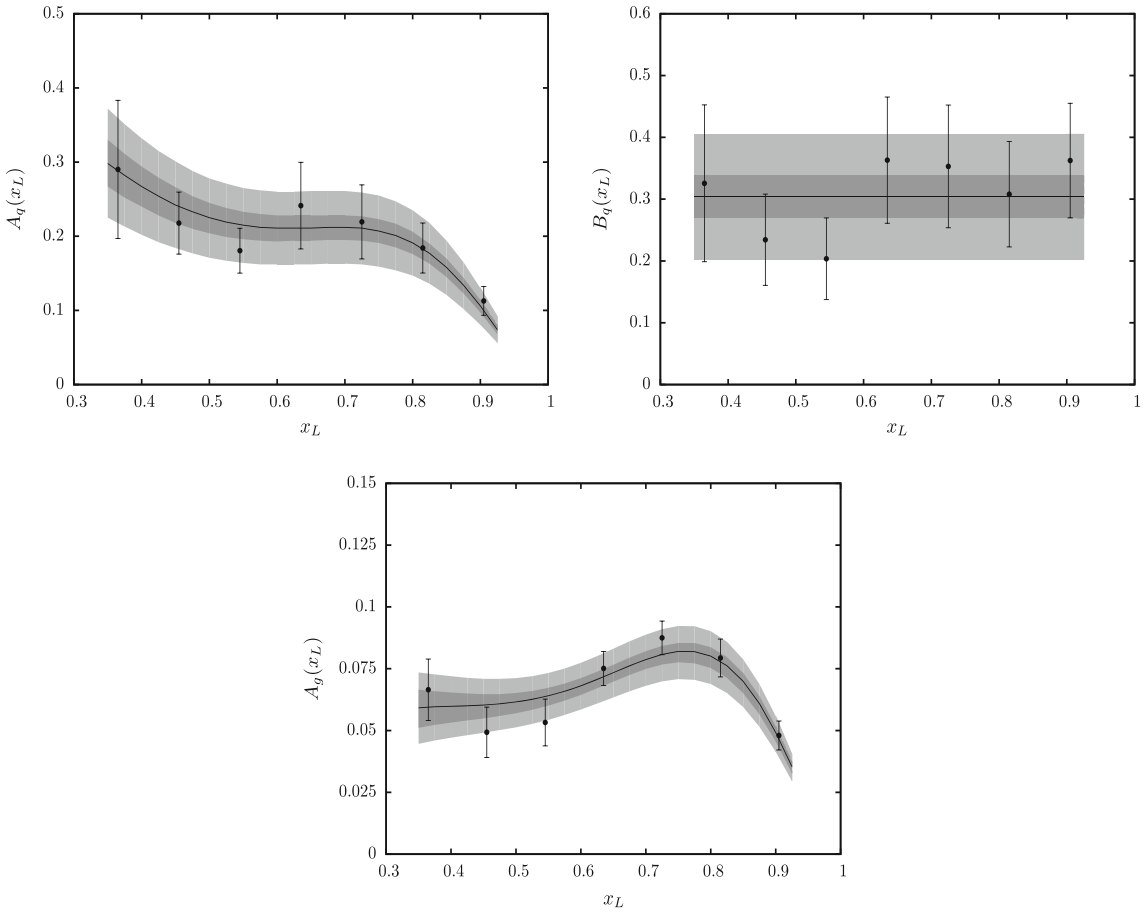

Fig. 1 The *black points* represent parameters A_q, B_q and A_g and their errors as a function of x_L, as obtained from fixed-x_L fits. The best fit parametrisations according to Eqs. (18–20) is displayed as a *black solid line*. The *dark and light grey bands* are obtained by propagating statistical and uncorrelated errors in the x_L-combined fit, as described in the text, with the condition $\Delta\chi^2 = 1$ and $\Delta\chi^2 = 9$, respectively

Table 3 Best fit parameter values and their errors

Parameters	$p_i \pm \delta p_i$
a_1	0.62 ± 0.07
c_1	17.2 ± 1.8
d_1	6.25 ± 0.17
e_1	1.77 ± 0.05
a_2	0.30 ± 0.03
a_3	0.32 ± 0.06
b_3	0.90 ± 0.27

inspecting Fig. 1. We adopt a redundant parametrisation of the coefficients of the type

$$A_q(x_L) = a_1\, x_L^{b_1}\,(1 + c_1\, x_L^{d_1})(1 - x_L)^{e_1}, \tag{14}$$

$$B_q(x_L) = a_2 + b_2\, x_L + c_2 x_L^2, \tag{15}$$

$$A_g(x_L) = a_3\, x_L^{b_3}\,(1 + c_3\, x_L^{d_3})(1 - x_L)^{e_3}, \tag{16}$$

where the term $1 + c\, x_L^d$ is included to describe the relative maximum of the normalisation A_q and A_g at intermediate values of x_L. For B_q we assumed a second order polynomial in x_L. The parameters $C_q = 0.5$, $C_g = 1$ and $B_g = 0$ are still kept fixed to the these values. All the QCD settings are the same as in fixed-x_L fits. With the help of Eq. (13) and Eqs. (14–16) we perform a series of x_L-combined fits. At each iteration we study the eigenvalues of the covariance matrix of the fit parameters. Small eigenvalues, in fact, are associated to (combination of) parameters which are loosely determined by data. We found that, at large x_L, both the singlet and the gluon normalisations can be described by a common parametrisation $g(x_L)$

$$g(x_L) = (1 + c_1\, x_L^{d_1})(1 - x_L)^{e_1}. \tag{17}$$

The B_q coefficient is found to be compatible with a constant so that only the parameter a_2 is left free to vary in the fit.

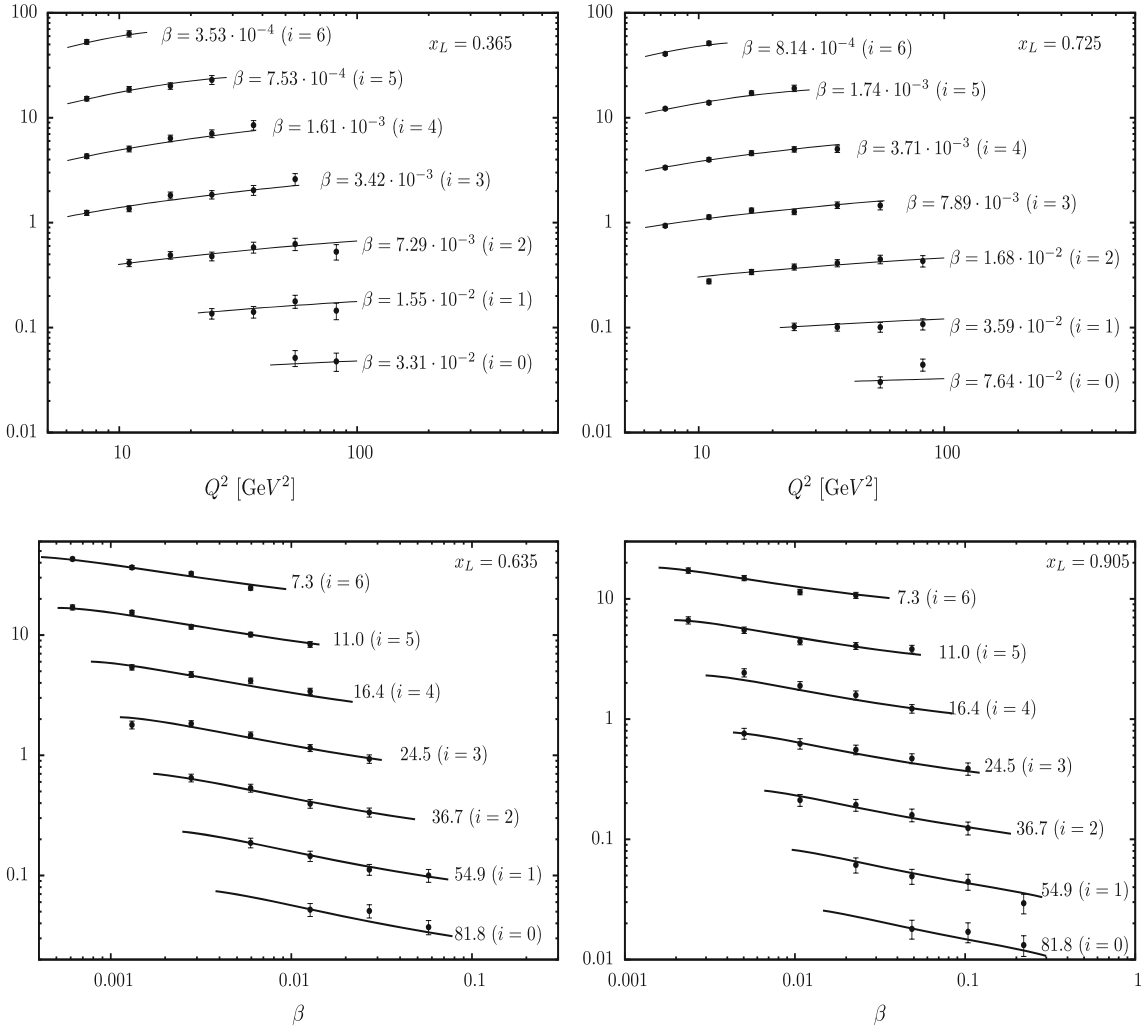

Fig. 2 *Top* reduced cross section as a function of Q^2 at different β in two bins of x_L. *Bottom* reduced cross section as a function of β at different Q^2 (in GeV^2 units) in two bins of x_L. The reduced cross section is scaled by a factor 3^i for better visibility. H1 points from Ref. [27]. The *error bars* associated with the data points show the sum in quadrature of the statistical and total systematic uncertainty

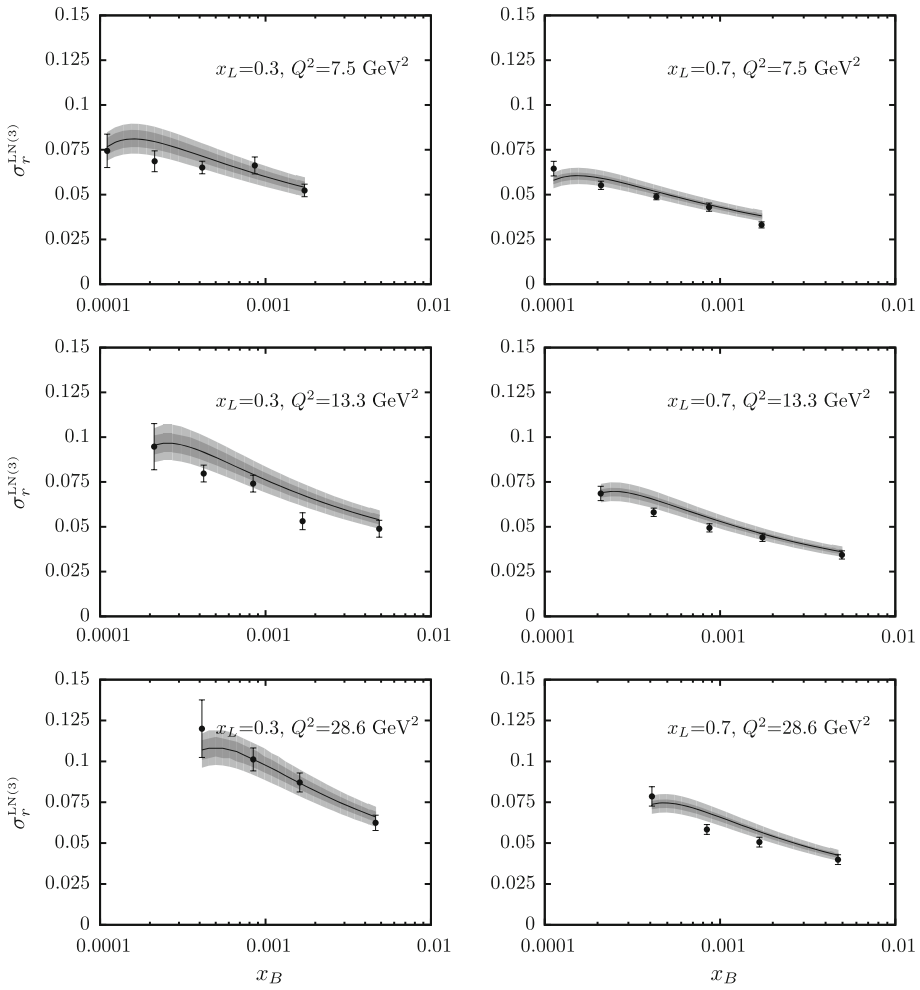

Fig. 3 Best fit predictions compared to ZEUS data [37]. The *error bars* associated with the data points show the sum in quadrature of the statistical and total systematic uncertainty. The *dark grey error band* corresponds to $\Delta\chi^2 = 9$ and it is constructed with $S_{k=1,\ldots,14}$. The *light grey error band* is constructed as the quadratic sum of statistical ($S_{k=1,\ldots,14}$) and systematic ($S_{k=15,\ldots,34}$) errors

Finally we found that b_1 is determined with rather large error and compatible with zero, so that we fix it to this value. The final form of the parametrisations of the coefficients is then

$$A_q(x_L) = a_1\, g(x_L), \tag{18}$$

$$B_q(x_L) = a_2, \tag{19}$$

$$A_g(x_L) = a_3\, x_L^{b_3}\, g(x_L), \tag{20}$$

for a total of seven free parameters. The best fit, with statistical and uncorrelated errors added in quadrature, returns a value of $\chi^2 = 143.6$ for 196 degrees of freedom. The resulting χ^2 in each x_L-bin is presented in Table 2. In the third column of the same table is indicated the increase of the χ^2 generated by the combination procedure in each x_L-bin with respect to the result presented for fixed-x_L fit in Table 1. Comparing the partial χ^2 for each value of x_L in Table 2 and Table 1 we conclude that the combined-x_L fit does not introduce any misrepresentation in the description of any given x_L bin. We further quantify the quality of the chosen coefficient parametrisations comparing the sum of the χ^2 obtained by fixed-x_L (134.8) with the χ^2 from the combined fit (143.6). The combination procedure induces an increase in the overall χ^2 of 8.8 units and, on average, around one unit across the x_L bins. The best fit parameters and relative errors are reported in Table 3. The best fit predictions are compared to H1 data in Fig. 2 in two representative bins, $x_L = 0.365$ and $x_L = 0.725$, respectively. From the plot it appears that the hard-scattering formula in Eq. (6) together with nFF initial conditions describe data down to the lowest accessible value of Q^2. This in turn implies also that, in the kinematical range covered by the experiment, no additional power-suppressed terms are required to describe the data. The presence of large and positive scale violations up to the largest parton fractional momentum, β, reveals the substantial contribution to $\sigma_r^{LN(3)}$ of the gluon nFF distribution induced by QCD evolution. As a final remark we note that the singlet and gluon normalisation coefficients, A_q and A_g, in Eq. (13), have a different behaviour at small x_L. This in turn implies a violation of the so-called proton-vertex factorisation. If this hypothesis is enforced, that is, if we set $b_1 = b_3$ and let this parameter free to vary in the fit, we obtain a $\chi^2 = 150$. Therefore, in the explored kinematical range and given the accuracy of the present data, proton-vertex factorisation holds to a good approximation.

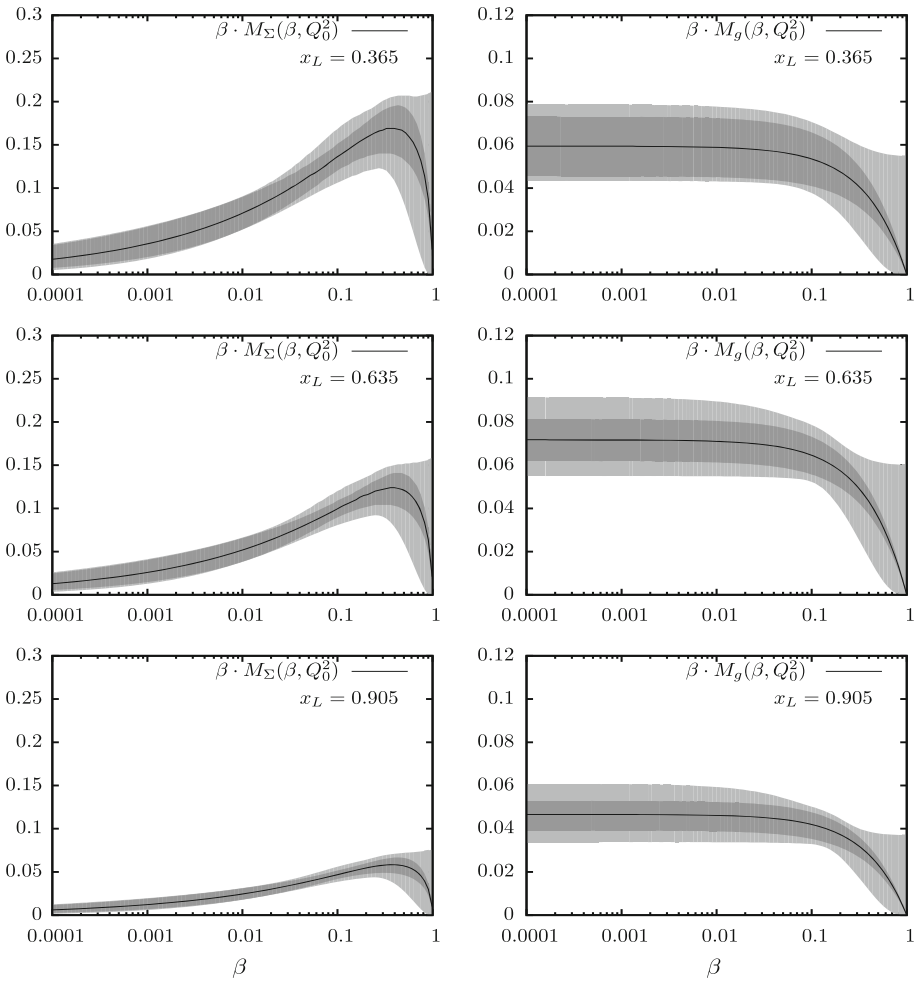

Fig. 4 Singlet (*left*) and gluon (*right*) momentum distributions at the initial scale $Q_0^2 = 1\ \text{GeV}^2$ in three representative bins of x_L. The *dark grey error band* is obtained with the $\Delta\chi^2 = 9$ criterion, while the *light grey one* with the additional $S_{k=35,\ldots,38}$ parametrisations added in quadrature

5 Error estimation and propagation

In order to judge the agreement with other data sets and observables or to assess effects beyond the ones taken into account by the theoretical model, the obtained nFF parametrisation must be supplemented, fully exploiting the potential of the data, by a careful error analysis. The general method with which experimental and theoretical uncertainties are propagated to a generic observable F is based on the construction of alternative nFFs parametrisation sets S_k. By defining the difference $r_k = F(S_k) - F(S_0)$ and indicating with S_0 the best fit parametrisation, the uncertainties on a F are given by

$$\Delta F^+ = \left[\sum_{k=1}^{n} r_k^2\, \theta\big(r_k\big)\right]^{1/2}, \quad \Delta F^- = \left[\sum_{k=1}^{n} r_k^2\, \theta\big(-r_k\big)\right]^{1/2}, \tag{21}$$

where θ is the Heaviside step function. In order to propagate statistical and uncorrelated uncertainties, following Refs. [34,35], we have diagonalised the covariance matrix of the best fit parameters and constructed a set of alternative parametrisations $S_{k=1,\ldots,14}$ according to the standard $\Delta\chi^2 = 1$ criterion. The error band constructed with the help of Eq. (21) and the $S_{k=1,\ldots,14}$ parametrisation set is shown in Fig. 1. The latter is narrower than individual errors on parameters obtained from fixed-x_L fits. This error reduction is in fact due to the x_L-combination, and can be understood considering for example B_q, which is just a constant as a function of x_L. In the combined fit, this parameter is constrained by 203 points rather than 29 of a single x_L bin and so it is determined far more precisely. Since,however, fixed-x_L fits, by construction, represent the best parametrisations of the data and Eqs. (18–20) are interpreted as a mere interpolating tool, we require that the accuracy of the x_L-combined fit does not exceeds the one of the fixed-x_L fits. We found that a conservative $\Delta\chi^2 = 9$ criterion matches these requirements, as shown in Fig. 1. We also note that, incidentally, this number is close to the combination penalty reported in Table 2.

We now turn to the inclusion of systematics in the error analysis. In data from Ref. [27] nine systematics sources are identified plus the luminosity uncertainty [36]. For each of them we performed, according to the so-called offset method, alternative fits in which each s_k is held fixed in turn either to -1 or $+1$ and produced the parametrisation set $S_{k=15,\ldots,34}$.

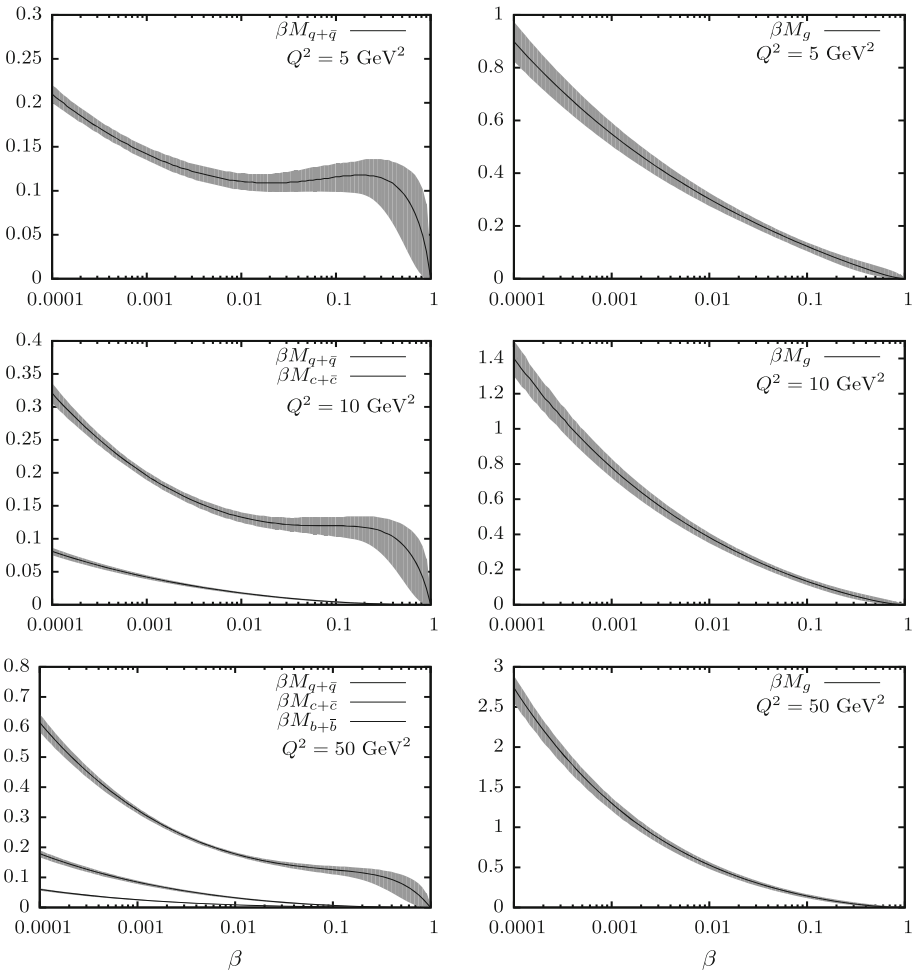

Fig. 5 Momentum distributions at various Q^2 at $x_L = 0.635$. The *error band*, corresponding to the $\Delta\chi^2 = 9$ criterion, is obtained with the $S_{k=1,\ldots,14}$ and $S_{k=35,\ldots,38}$ parametrisations added in quadrature

For some sources, for example the 5 % luminosity uncertainty common to all data points, the shifts induce steady variation of the χ^2 and mostly correlates with the central values of the normalisations coefficients a_1 and a_3. The impact of the propagation of systematic errors are presented in Fig. 3 where the best fit predictions are compared to ZEUS data [37]. The latter are presented in terms of reduced cross sections as a function of x_B in different bins of x_L and Q^2 and integrated up to the same $p_{T,\max} = 0.2$ GeV, as in the H1 analysis from which nFFs are obtained. The effects induced by systematic errors are significant, as shown by the light grey band in Fig. 3. After taking into account all error sources we find that predictions based on nFFs describe ZEUS data both in shape and normalisation.

We conclude this section attempting an estimate of theoretical errors. Among them we mention the ones related to pQCD settings and the ones related to the choice of the parametrisation of initial conditions. The latter are by far dominant in the present analysis so we focus on them in the following. The impact of the functional form used for the x_L-combination is estimated in 8.8 χ^2 units, which corresponds to the combination penalty term. The uncertainties associated to the functional forms chosen for the β dependence are not so easily quantified. In the following we restrict ourselves to study the impact of the main assumptions in the parametrisation of the initial conditions at large β. The parameters controlling the large-β behaviour, being almost unconstrained by the data, were held fixed in the fit, i.e. $C_q = 0.5$ and $C_g = 1$. This implies that the error propagation produces, as shown in Fig. 4, an artificial shrinkage of the (dark grey) error band at large β and by no means represents a correct error estimate in this limit. In order to quantify the errors introduced by these assumptions, we performed four additional fits in which the C_q and C_g parameters are kept fixed in the minimisation but chosen in the following combinations: $(C_q, C_g) = (0, 1), (2, 1), (0.5, 0), (0.5, 3)$. The latter values are chosen so that fits return a difference of around $\Delta\chi^2 = 9$ with respect to best fit. The latter four alternative parametrisations, $S_{k=35,\ldots,38}$, are used to produce the light grey error band shown in Fig. 4 and shows the degree of underdetermination of the distributions in this region. These additional parametrisations can be especially useful to propagate uncertainties to observables which require nFFs large-β extrapolation, for example jet cross section. Less problem-

atic appear the Q^2 extrapolation, since the latter is fully predicted by the theory. In Fig. 5 we present the initial condition at $x_L = 0.635$ for three different values of Q^2. It is interesting to note that the uncertainties on the nFFs increase as Q^2 decrease. This effect can be partly ascribed to the fact that no data point with Q^2 below 7.3 GeV^2 is included in the fit. But, more importantly, it has to be ascribed to QCD evolution: small displacements of the parametrisations at high Q^2, where they are actually constrained by the data, turn into large fluctuations of the initial conditions at Q_0^2, due to the logarithmic nature of QCD evolution equations.

6 Conclusions

In this paper we have presented a perturbative QCD analysis and extraction of neutron fracture functions from forward neutron production in DIS in HERA kinematics. Data can be described by the leading-twist approximation implied by the hard-scattering factorisation formula and perturbative QCD evolution down to the lowest values of Q^2 accessed by the experiment. The results of the fit and within the precision of the present data, indicate that the proton-vertex factorisation hypothesis is supported to good accuracy, a fact which is likely to be related to the relative low β regime accessed by the measurements. The nFFs low-Q^2 extrapolation, although with large uncertainties, can be used to address the impact of absorptive effects going from the DIS to the photoproduction regime. The predictions based on the obtained nFFs have been successfully compared to ZEUS data and an error estimation on nFFs has been provided. The obtained NLO QCD nFFs parametrisation is a quantitative tools which can be used in factorisation tests in processes with a tagged forward neutron. In this context we mention dijet photoproduction in ep collisions and dijet or Drell–Yan pair production in hadronic collisions. For the latter process, next-to-leading order corrections have been estimated in Refs. [38,39]. The nFFs parametrisation and error set are available upon request to the author and are provided as Fortran steering file for the `QCDNUM17` package.

Acknowledgments We warmly thank Armen Bunyatyan and Vitaly Dodonov for numerous discussions on the measurements and for providing us the breakdown of the systematics errors.

References

1. M. Basile et al., Nuovo Cim. A **66**, 129 (1981)
2. R.P. Feynman, Phys. Rev. Lett. **23**, 1415 (1969)
3. J. Benecke et al., Phys. Rev. **188**, 2159 (1969)
4. J.C. Collins, Phys. Rev. D **57**, 3051 (1998)
5. J.C. Collins, Phys. Rev. D **61**, 019902 (2000)
6. J.C. Collins, J. Phys. G **28**, 1069 (2002)
7. M. Grazzini, L. Trentadue, G. Veneziano, Nucl. Phys. B **519**, 394 (1998)
8. L. Trentadue, G. Veneziano, Phys. Lett. B **323**, 201 (1994)
9. YuL Dokshitzer, Sov. Phys. JETP **46**, 641 (1977)
10. V.N. Gribov, L.N. Lipatov, Sov. J. Nucl. Phys. **15**, 438 (1972)
11. G. Altarelli, G. Parisi, Nucl. Phys. B **126**, 298 (1977)
12. D. Graudenz, Nucl. Phys. B **432**, 351 (1994)
13. F. Ceccopieri, D. Mancusi, Eur. Phys. J. C **73**, 2435 (2013)
14. V. Andreev et al. (H1 Collaboration), DESY-14-035. e-Print: arXiv:1404.0201 [hep-ex]
15. S. Chekanov et al., ZEUS Collaboration. Nucl. Phys. B **776**, 1 (2007)
16. T.T. Chou, C.N. Yang, Phys. Rev. D **50**, 590 (1994)
17. A.B. Kaidalov et al., Eur. Phys. J. C **47**, 385 (2006)
18. B.Z. Kopeliovich et al., Phys. Rev. D **85**, 114025 (2012)
19. N.N. Nikolaev, J. Speth, B.G. Zakharov (1997). hep-ph/9708290
20. U.D. Alesio, H.J. Pirner, Eur. Phys. J. A **7**, 109 (2000)
21. V.A. Khoze, A.D. Martin, M.G. Ryskin, Eur. Phys. J. C **48**, 797 (2006)
22. M. Bishari, Phys. Lett. B **38**, 510 (1972)
23. H. Holtmann et al., Phys. Lett. B **338**, 363 (1994)
24. M. Klasen, G. Kramer, Eur. Phys. J. C **49**, 957 (2007)
25. S. Chekanov et al., ZEUS Collaboration. Nucl. Phys. B **827**, 1 (2010)
26. A. Aktas et al., H1 Collaboration. Eur. Phys. J. C **41**, 273 (2005)
27. F.D. Aaron et al., H1 Collaboration. Eur. Phys. J. C **68**, 381 (2010)
28. G. Camici, M. Grazzini, L. Trentadue, Phys. Lett. B **439**, 382 (1998)
29. F.A. Ceccopieri, L. Trentadue, Phys. Lett. B **655**, 15 (2007)
30. F.A. Ceccopieri, L. Favart. arXiv:1205.6356
31. M. Botje, Comput. Phys. Commun. **182**, 490 (2011)
32. F. James, M. Roos, Comput. Phys. Commun. **10**, 343 (1975)
33. C. Pascaud, F. Zomer, LAL-95-05
34. J. Pumplin et al., Phys. Rev. D **65**, 014013 (2001)
35. D. Stump et al., Phys. Rev. D **65**, 014012 (2002)
36. A. Bunyatyan, V. Dodonov, private communication
37. S. Chekanov et al., ZEUS Collaboration. Nucl. Phys. B **637**, 3 (2002)
38. F.A. Ceccopieri, L. Trentadue, Phys. Lett. B **668**, 319 (2008)
39. F.A. Ceccopieri, Phys. Lett. B **703**, 491 (2011)